Obrabotka metallov (tekhnologiya, oborudovanie, instrumenty) = Metal Working and Material Science. 2026 vol. 28 no. 1 pp. 275–294
ISSN: 1994-6309 (print) / 2541-819X (online)
DOI: 10.17212/1994-6309-2026-28.1-275-294

NSTU NETI

Obrabotka metallov - Metal Working and Material Science

Journal homepage: http://journals.nstu.ru/obrabotka_metallov

Study of abrasive wear resistance of low-carbon steel surface-alloyed with the Fe-C-Cr system using gas tungsten arc welding (GTAW)

Yulia Karlina [1, a, *], ***Vladimir Konyukhov*** [2, 3, b], ***Tatiana Oparina*** [2, c]

[1] National Research Moscow State University of Civil Engineering, 26 Yaroslavskoe Shosse, Moscow, 129337, Russian Federation
[2] Irkutsk National Research Technical University, 83 Lermontova str., Irkutsk, 664074, Russian Federation
[3] Cherepovets State University, 5 Lunacharsky pr., Cherepovets, 162600, Russian Federation

[a] https://orcid.org/0000-0001-6519-561X, jul.karlina@gmail.com; [b] https://orcid.org/0000-0001-9137-9404, konyukhov_vyu@mail.ru;
[c] https://orcid.org/0000-0002-9062-6554, martusina2@yandex.ru

ARTICLE INFO

Article history:
Received: 13 December 2025
Revised: 06 January 2026
Accepted: 22 January 2026
Available online: 15 March 2026

Keywords:
Chromium carbides
Alloying
Welding arc
Voltage
Wear
Coating

ABSTRACT

Introduction. The surface properties of machine parts and tools play a significant role in their performance when the interactive mechanical action on the metal surface leads to wear. Modifying the surface properties of components is essential, particularly in critical industrial applications. Surface properties such as hardness and wear resistance of a metallic material can be primarily enhanced either by introducing a new phase or element into the surface layer, or by surface treatment (e.g., laser, plasma, or electron beam) of the base material to develop the desired phases within the matrix. Gas tungsten arc welding (*GTAW*) offers several advantages over other methods, primarily in terms of precision, speed, and versatility at a relatively low cost. Technically, it is capable of alloying the metal surface more quickly and uniformly compared to conventional carburizing and nitriding processes. During arc heating, the surface is modified by melting a paste or coating preapplied to the substrate through the rapid application of intense arc heat. This results in a steep thermal gradient accompanied by high heating and cooling rates, similar to the principles of laser and electron beam cladding. ***The objective*** of the present study is to evaluate the feasibility of surface alloying of low-carbon steel with the *Fe–C–Cr* system using gas tungsten arc welding (*GTAW*). **Methods.** The paper examines low-carbon steels using *St3* steel as an example. The steel served as the substrate and was coated with a layer (≤1 mm thick) in experiments employing the *Fe–C–Cr* surface alloying method via *GTAW*. A powder mixture of *Fe* and Cr_2O_3 was used as the coating alloy, with a particle size of 45 μm. The samples were examined using optical and electron microscopy, as well as X-ray diffraction. Abrasion resistance tests were also conducted. **Results and discussion.** Our research has shown that during gas tungsten arc welding (*GTAW*), when melting a *Fe–C–Cr* paste, the shape and size of the fusion zone (*FZ*) on the steel surface are determined by arc parameters such as current, voltage, and travel speed, while the molten metal pool is protected from atmospheric contamination by an inert argon shielding gas. Adding carbon dioxide to the shielding gas increases the arc's heat input. To produce a series of hypereutectic hardfaced surface layers using the *Fe–C–Cr* system, paste variants with varying carbon and chromium contents were developed to study their microstructure, wear resistance, and wear mechanism. Positive results were obtained, demonstrating a two- to three-fold increase in abrasive wear resistance.

For citation: Karlina Yu.I., Konyukhov V.Yu., Oparina T.A. Study of abrasive wear resistance of low-carbon steel surface-alloyed with the Fe-C-Cr system using gas tungsten arc welding (GTAW). *Obrabotka metallov (tekhnologiya, oborudovanie, instrumenty) = Metal Working and Material Science*, 2026, vol. 28, no 1, pp. 275–294. DOI: 10.17212/1994-6309-2026-28.1-275-294. (In Russian).

Introduction

The loss of material due to wear is the main problem faced by agricultural, mining, earth-moving equipment, and other machine parts [1, 2]. Reducing wear and extending the service life of machine parts and mechanisms is at the heart of many resource-based industries that rely heavily on wear-resistant materials for mining and processing, as equipment must withstand particularly aggressive conditions that require resistance to abrasion, corrosion, and erosion. In [1], the author provides a figure for the estimated cost of

*** Corresponding author**
Karlina Yulia I., Ph.D. (Engineering), Research Associate
National Research Moscow State Construction University,
26 Yaroslavskoe shosse,
129337, Moscow, Russian Federation
Tel.: +7 914 879-85-05, **e-mail:** jul.karlina@gmail.com

depreciation for the Canadian industry, estimating it at 2.5 billion dollars per year. At oil sands production facilities in Northern Alberta, the cost of downtime for any of the production lines is estimated at 3–6 million dollars per day [1]. For a typical oil sands operator, it costs more than 40 million dollars per year to replace worn parts and pay for labor. Similar situations can be found in the mining, pulp and paper industry**,** and other industries, not only abroad, but also in Russia. It is known that the key to maximizing the reliability and uptime of machine parts and mechanisms is to apply wear-resistant and cost-effective coatings. The use of an advanced wear-resistant coating on top of a conventional steel component or substrate provides significant savings in terms of material cost and manufacturability.

In this regard, to increase the wear resistance and corrosion resistance of machine parts and mechanisms, various methods of restoring the geometric dimensions of a worn part and subsequent hardening are usually used, such as welding, thermal spraying, surfacing, electrodeposition , and vapor deposition — applying highly wear-resistant materials to the surface of components [3–4]. Arc and plasma surfacing technology encompasses a wide range of processes for applying wear-resistant hard materials [1, 2].

Self-shielded flux-cored arc welding (*FCAW*), which does not require additional shielding gas, is a widely used surfacing technology due to a number of advantages such as a continuous process and suitability for all welding positions and part sizes.

Wear resistance is mainly attributed to the primary chromium carbide formed during solidification in welding [1, 2, 3]. It has been shown that the rapid heating and cooling cycles characteristic of welding operations affect the morphology of the resulting microstructures. Primary carbides form hexagonal rods (M_7C_3) and a eutectic phase consisting of austenite and small rods of M_7C_3 carbides [5–8]. *C*, *Mn*, *Cr*, *Mo*, *Cu*, *Ni*, *Co*, *V*, *Ti*, *W*, *Nb*, and *B* are used as alloying elements for iron-based surfacing materials [1, 2]. Depending on the constituent alloying elements, they form one or more microstructures, including austenite, ferrite, martensite, and carbides [1, 2]. Iron-based surfacing alloys with a high content of *Cr* and *Mo* contribute to the formation of hard carbide and boride phases, which increases their abrasion resistance. These alloys can have various matrix structures, including austenitic, martensitic, pearlitic, ferritic, or a combination of these structures. Some iron-based alloys, such as high-chromium carbides, may exhibit transverse surface cracks in the deposited layers [1]. Despite these cracks, or “stress relief” cracks, the deposited layers are suitable for many applications in the mining and earth-moving industries.

Surface hardening technologies using a laser [2, 3], an electron beam [9–13], and a plasma arc [14–19] as heating sources are used to increase the hardness and wear resistance of machine parts and tools. Currently, many technological methods of surface treatment of metals have been developed, such as solid and liquid state quenching, and alloying in the solid, liquid, and gaseous states [2, 6–8, 14–19]. In order to obtain high hardness during surface alloying, materials with high hardness, such as carbides, are used. The concept of surface alloying of metals with concentrated energy sources (laser, electron beam, plasma) was initially implemented through the use of various coatings based on one or more alloying elements (*C*, *Cr*, *W*, *Ti*, etc.) in a system with a base component. It was found that in this way, various combinations of alloying elements with the required amount of carbon can be applied and incorporated into steel surfaces and surface layers of the metal [6–8, 14, 15].

In the first stage of surface treatment with concentrated energy sources (laser, electron beam, plasma arc), saturation of the surface with an alloying element can be achieved by two different mechanisms: (a) surface alloying, which involves melting the surface layer so that the base alloying element and carbon enter the liquid phase; and (b) solid-state diffusion of carbon activated by heating. Surface alloying by melting has been experimentally demonstrated for various substrates and alloying elements. Most of the published works concerning surface carburizing [20–22], boriding [23–25], chromizing [26–28], and nitriding of steels [25, 29–31] have achieved this using this mechanism. Although each of the above surface alloying processes has its advantages and disadvantages, it is necessary to choose the most appropriate coating process based on the requirements of the hardening coating and the application area. The choice of a technological process using concentrated heating sources for applying a hardening coating depends on various factors, such as the deposition rate, the cost of surfacing, residual stresses and deformations, as well as the requirements for heat treatment of the substrate itself. Other important factors include the

size of the weld bead and the requirements for dilution with the substrate, the type of consumables, the size and shape of the welded component, automation requirements, portability of welding equipment, and surface finishing requirements. The latter requirement is very important, since the surface of machine parts and tools obtained from surfacing or alloying exhibits high hardness, which significantly complicates final machining.

It is known that alloys of the *Fe–Cr–C* alloying system, as a rule, have a high initial carbon content, which leads to a high content of primary carbides $(Fe,Cr)_7C_3$ and high wear resistance [11–12]. Experimental studies have shown that with an increase in the *Ti* content, primary $\boldsymbol{M_7C_3}$ carbides are refined, and the dispersion of the *TiC* solid phase improves wear resistance [6–12]. In the process of surface carburizing, the amount of carbon introduced by the melting mechanism is sometimes so large that even hypereutectic compositions (>4.3 wt.% *C*) produce carburized layers [32–34]. However, repeated hardening of the substrate leads to the formation of cracks, which is a significant disadvantage of the process and is explained by the inherently brittle nature of the resulting microstructures, a condition promoted by extremely high cooling and solidification rates. Another disadvantage of the process is the formation of gas porosity in the hardened surface layers.

In most works on surfacing with solid and flux-cored wires, it is noted that in order to enhance the completeness of metallurgical reactions in the molten weld pool, which consists of an "*Fe–C* + alloying element" system, it is necessary to increase the heat content of the welding arc, which is achieved by using a mixture of molecular gases [35–38]. Similar recommendations are given by the authors of works on plasma and argon-arc carburizing of steels using pastes and coatings applied to the surface of the workpiece [14, 18, 19].

In addition to this fact, it is necessary to understand that the diffusion of dissolved elements, especially carbide-forming elements, during solidification is one of the most important factors affecting the segregation and precipitation of carbides. In modeling works [39–41] based on the iron-carbon and iron-chromium-carbon phase diagrams, the role of the solute solidification rate in the alloying process was noted. Energy density and heat input also play an important role in the processes of laser alloying of steel and alloys [38–42].

It is known from [39–44] that high matrix hardness is also necessary to ensure high wear resistance of the coating. To achieve high wear resistance, the hardness of the deposited or alloyed layer must be higher than the hardness of the abrasive particles [6, 45].

The hardness of primary carbides $(Fe,Cr)_7C_3$ in *Fe–Cr–C* alloys is usually close to 1,500 HV, which is higher than that of Fe_3C (1,000–1,100 HV) [5, 46]. Primary carbides are known for their strong covalent bond and high temperature stability, but, unfortunately, they are quite brittle due to their high hardness [8, 47]. Coatings [1, 48] containing a high proportion of carbides with a hardness higher than that of abrasive particles can effectively resist abrasion. Ledeburitic materials [17, 49] can have higher wear resistance due to their microstructure and higher hardness, while austenitic transformation occurring during heat treatment can also affect hardness and, as a result, abrasive wear resistance [13, 50]. Some authors have tested surface-alloyed steels obtained by gas tungsten arc welding **(*GTAW*)** with an austenitic structure to achieve improved wear resistance characteristics [17, 18, 43–47]. Complex multicomponent compositions of pastes, coatings**,** and filler rods for surface carburizing of steels were considered.

Developing this direction, it is possible to use simple mixtures of the *Fe–Cr–C* alloying system, for example, based on chromium oxide and graphite, which do not require significant manufacturing costs, such as for welding electrodes or flux-cored wires. Chromium oxide forms a wide range of oxide phases, for example, *CrO*, CrO_2, Cr_2O_3, Cr_3O_4, etc. Among these phases, **α**-Cr_2O_3 is the most stable form**,** having a corundum structure (a = 4.96 Å, c = 13.59 Å, c/a = 2.74) and, in combination with a graphite and iron powder composition, has not previously been used.

Therefore, in this work, instead of the diffusion process of saturating the surface layer with carbon, surface alloying with chromium using chromium oxide and graphite was studied by melting a coating previously applied to the metal surface.

The purpose of the work is to evaluate the possibility of surface alloying of low-carbon steel with the *Fe–Cr–C* system using gas tungsten arc welding (*GTAW*).

To achieve this purpose, the following ***tasks*** were addressed:

– the influence of the technological parameters of the process on the depth of the alloyed layer produced by the *Fe–Cr–C* system was evaluated;

– the structure of the surface layer obtained by surface alloying and its hardness were investigated;

– an evaluation of the abrasive wear resistance of the alloyed layer produced by the *Fe–Cr–C* system was carried out.

Materials and methods of research

The base material used in the experiment was low-carbon *St3* steel with sample dimensions of 100 mm × 50 mm × 10 mm, which was used as substrates and on the surface of which a coating (no more than 1 mm thick) was applied in experiments using the *Fe–Cr–C* surface alloying method with gas tungsten arc welding (*GTAW*). This *St3* steel was chosen as a model system to facilitate distinguishing between the alloyed layer based on *Fe–Cr–C* and the base metal of the substrate in terms of microstructure and mechanical properties. A powder mixture of *Fe* and Cr_2O_3 powders was used as the coating alloy (Table). The particle size was 45–60 μm.

Composition of alloy paste

No.	Graphite (wt.%)	Chromium, Cr_2O_3 (wt.%)
1	10	90
2	15	85
3	20	80

Chromizing was carried out in two stages. At the first stage, the outer surface of the substrate material was coated with a paste containing *Fe–Cr–C* mixed with a dilute solution of polyvinyl alcohol. The thickness of the paste ranged from 200 to 230 μm. It was measured with a coating thickness gauge using magnetic induction and eddy current methods. At the second stage, the surface of the coated samples was re-melted with a welding arc. For the experiments, tungsten arc treatment in an argon atmosphere with direct current was used. The electrode was 2% thoriated tungsten; the nozzle diameter was 11 mm. The arc power ranged from 2 to 5 kW, and the travel speed ranged from 1.5 to 5 mm/s. In the process of re-melting the coating and the surface layer of the metal, a constant current and voltage regime was implemented. The formation of a protective atmosphere was ensured by the continuous supply of argon to the arc formation zone. The geometry of the "weld pool" contributed to the complete melting of the substrate together with the applied paste. The diameter of the electrode in all experiments was 2.4 mm. Argon flow rate was 12 L/min; the distance between the torch nozzle and the coated surface was 3–5 mm. The gas mixture consisted of 90% argon and 10% CO_2. The gases were mixed with a standard mixer. The current and voltage parameters were recorded by a *RADS01* argon arc welding parameter recorder.

The microstructures of the polished and etched cross-sections of the samples were observed using an optical microscope (*OM*) and a *Tescan Vega* scanning electron microscope (*SEM*). After the above processes, the samples were cut perpendicular to the treated surface, across the resulting tracks. Samples of cross-sections of alloyed layers for observation in *OM* and *SEM* were prepared in a plane perpendicular to the scanning direction. Metallographic studies were then performed. The samples were polished using abrasive paper of various grit sizes, and finally with Al_2O_3. Microhardness profiles for the studied layers were determined in polished cross sections of the samples. The microhardness was measured using the *Vickers* method. The tests were carried out at a load of $\boldsymbol{P}$ = 0.1 kgf (≈ 0.981 N).

The characteristic diffraction crystal planes of the samples were studied using an *X'Pert PRO* X-ray diffractometer (*XRD*) (*PANalytical*, The Netherlands) under various processing parameters. When measuring the full width at half maximum (*FWHM*), *Cu-Kα* radiation was used; the operating voltage was 40 kV, the operating current was 40 mA, and the scanning angle range was 5–80°.

Tests for abrasive wear were carried out using fixed abrasives**,** as regulated by *GOST 17367-71*.

Research results

At the first stage of the research, the arc voltages in argon and argon–carbon dioxide mixtures were measured. A pure argon welding arc is characterized by a soft, flexible arc at a relatively low voltage (approximately 16–21 V) in the welding current range of 50–100 A (Fig. 1). An increase in the proportion of active CO_2 gas in the range of 5–10% increases the arc voltage, makes it more constricted, and increases the penetration depth. It can be seen that at direct current, the arc voltage increases with increasing CO_2 content, and the arc voltage–current curve "shifts upward"**.** As the flow rate of active CO_2 gas in the mixture increases, the arc voltage increases (Fig. 1, *b*). This fact is associated with the high thermal conductivity of CO_2, necessitating higher voltages at the same current level to initiate and stabilize the arc. When using a gas mixture, the maximum temperature increases [1, 2], and the heat output of the arc increases (Fig. 1, *c*, *d*). This is due to the fact that the specific heat of the $Ar–CO_2$ mixture is higher than that of pure argon [13–18].

Fig. 2 shows the results for the depth of treatment when using pure argon and an argon–carbon dioxide mixture. It can be seen that the total depth of the affected surface layer increases with the addition of carbon

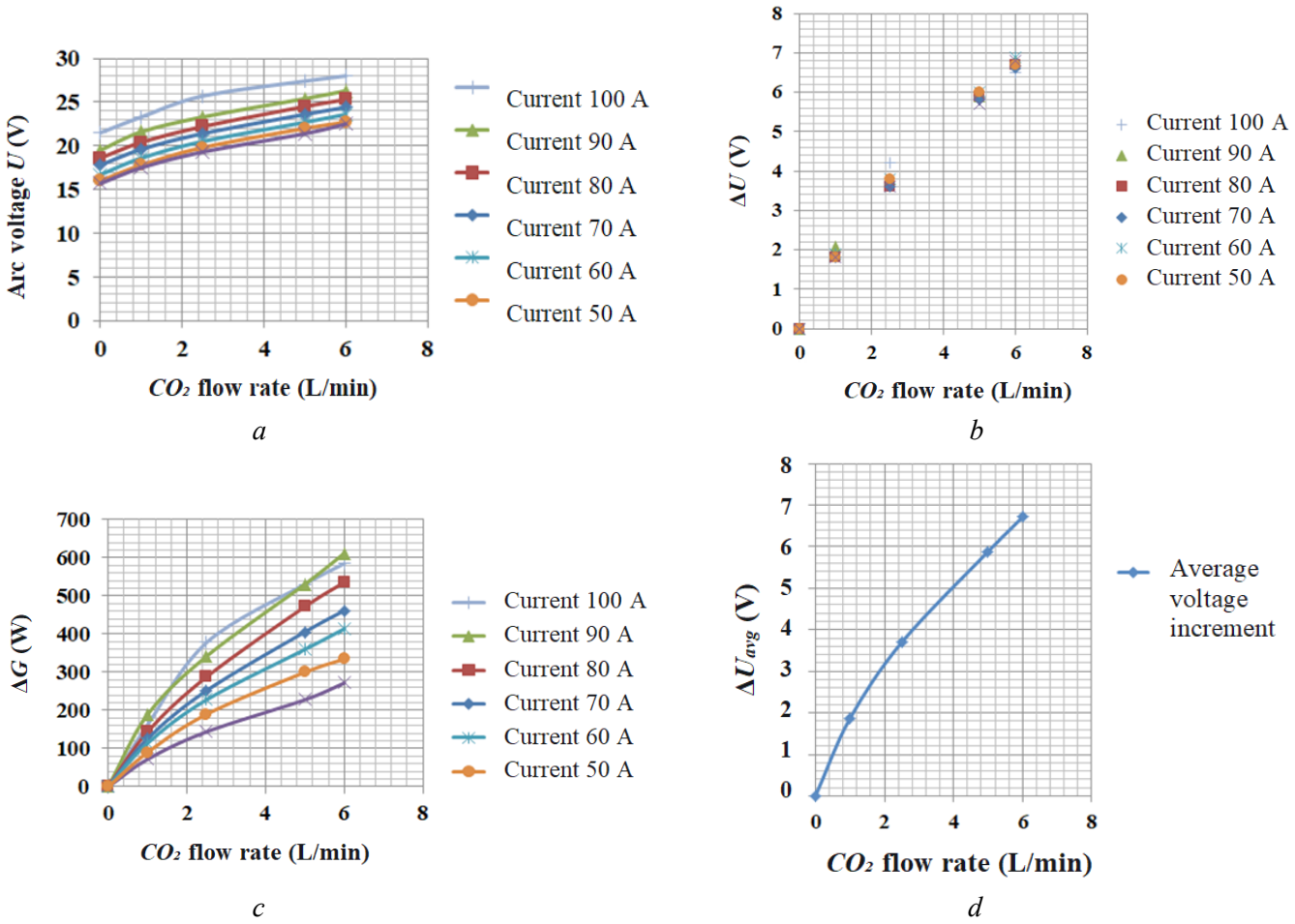

Fig. 1. Experimental results of welding arc parameter measurements:
a – dependence of voltage on CO_2 consumption; *b* – dependence of voltage increment on CO_2 consumption; *c* – dependence of arc power increment on CO_2 consumption; *d* – dependence of average voltage increment values on CO_2 consumption

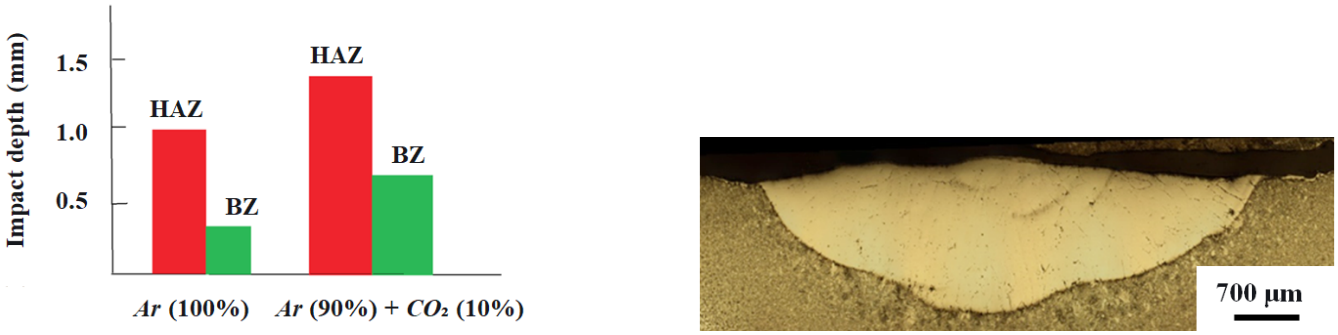

a *b*

Fig. 2. Changes in penetration depth depending on the composition of the shielding gas: *a* – histogram of changes in penetration depth; *b* – macrograph of the alloyed layer cross-section

dioxide to the mixture (the depth measurement error was 0.2 mm). The thickness of the alloyed layer varies from 150 to 1,000 μm. The difference in the thickness of the alloyed layer, despite the use of an identical pre-applied powder layer, occurs due to the use of different (and optimal) welding arc power levels (current from 50 to 100 A) and travel speed combinations. However, in our further work on surface alloying, we will refine the processing parameter ranges while developing the optimal conditions.

The surface layer consists of a fusion zone (*FZ*) and a heat-affected zone (*HAZ*) (Fig. 2, *b*). In Fig. 2, *b*, the fusion zone (re-melted region) is clearly visible on the transverse section in the form of a white layer.

Fig. 3 shows the microstructures of the alloyed layer formed on *St3* steel. Continuous alloyed layers were obtained on the surface as shown in Fig. 2, *b*. Two zones were observed in the microstructure: the surface layer was a fusion zone (re-melted region) as a result of the welding arc, and the substrate was heated below the melting point of the metal, thus undergoing phase and structural transformations according to the classical heat treatment scheme. The chromium-alloyed surface layer of the metal is clearly visible (white) on the cross section of the microsection (Fig. 2, *b*), which is immediately followed by a fusion line and a dark etched heat-affected zone. It should be noted that the alloyed layer–*HAZ* interface marks the melting limit (solid–liquid interface) and, therefore, is sharp. The area at the bottom of the micrograph shows the base metal that was not affected by the process. This sequence of zones was observed in all samples treated with the welding arc in our work. The fusion zone had a composite microstructure consisting of solid carbide phases (Fig. 4, *a*). Since carbon steel was used as the substrate, in addition to chromium and carbon, iron was also added to the deposited layer to form *Fe–Cr–C* alloys. Fig. 4 shows the X-ray diffraction spectra of the obtained alloys. The phase composition of the low-carbon alloy (composition **1**, Table) included a *Cr–Fe* solid solution (**α**-phase) and $(Cr,Fe)_{23}C_6$ carbide with a complex face-centered cubic

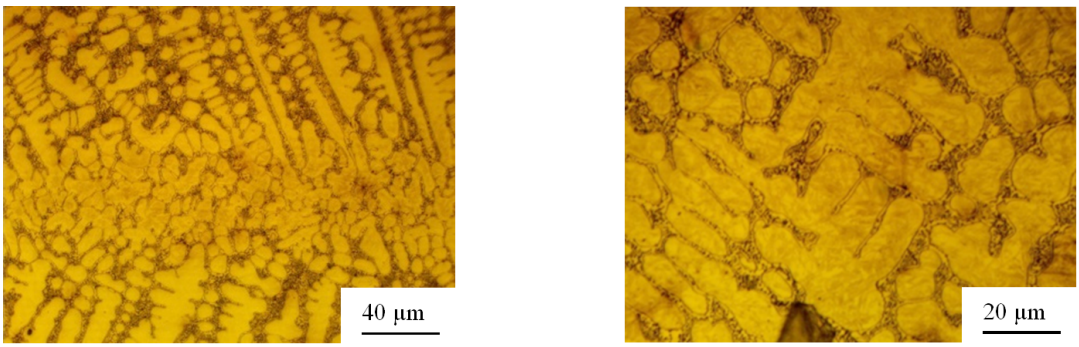

a *b*

Fig. 3. Primary carbide dendrites in the alloyed layer of composition **1**, at different magnifications

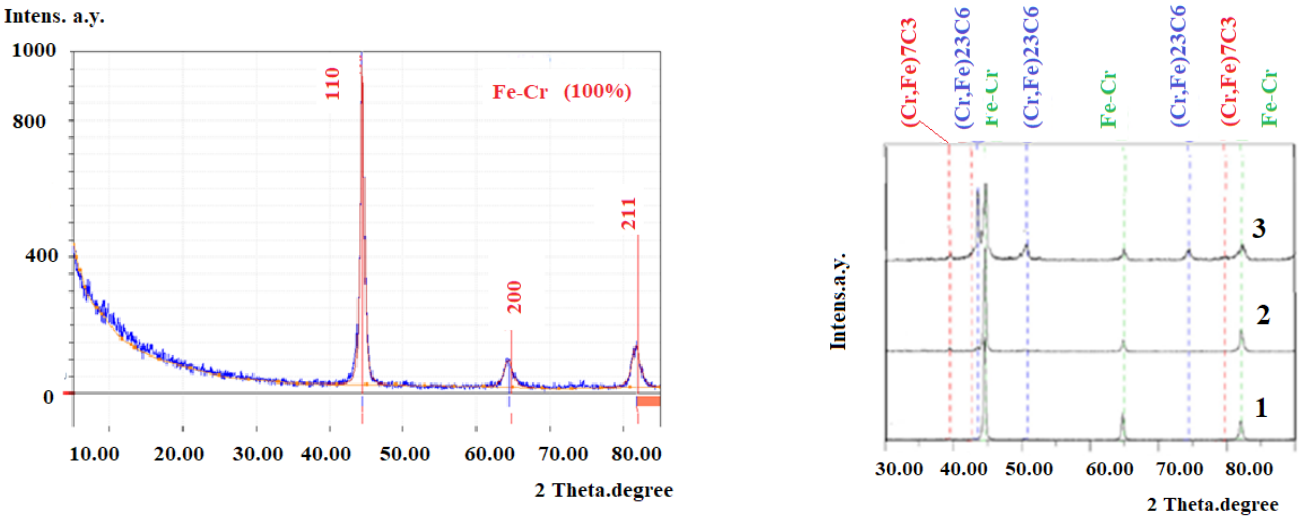

a *b*

Fig. 4. X-ray diffraction spectra of the obtained alloyed layers:
a – composition 1; *b* – combined spectra (compositions **1**, **2**, and **3**)

crystal structure. In the medium-carbon and high-carbon alloys (compositions **2** and **3**, respectively), the main identified phases were a *Cr–Fe* solid solution (**α**-phase) and $(Cr,Fe)_{23}C_6$ and $(Cr,Fe)_7C_3$ carbides with a hexagonal crystal structure.

The effect of various graphite additions in the filler material on the microstructure of the hardening coating can be seen in Fig. 5 using electron microscopy. During the solidification process, primary carbides $(Cr,Fe)_7C_3$ are formed, followed by the eutectic reaction [$L \rightarrow$ Cr–Fe + $(Cr,Fe)_7C_3$]. As a result, primary carbides $(Cr,Fe)_7C_3$ and eutectic colonies of *Cr–Fe* + $(Cr,Fe)_7C_3$ are formed in all hardening alloys. Moreover, the proportion of primary carbides $(Cr,Fe)_7C_3$ increases as the graphite addition increases from 10 to 20 wt.%, and the proportion of eutectic colonies of *Cr–Fe* + $(Cr,Fe)_7C_3$ decreases. The addition of graphite can increase the driving force for the formation of carbides (Fig. 5).

It was reported in the works of many authors [6–12] that the *C* content can change the microstructure and phase composition of *Fe–Cr–C* alloys. In this regard, considering our alloying compositions (graphite + chromium oxide according to Table), it can be predicted that a higher graphite content of graphite, and therefore carbon, contributes to a higher nucleation rate of primary chromium carbides, and their growth orientation tends to become more diverse [24–28]. In addition, the undercooling of the solid–liquid interface decreased as the latent heat of solidification was released. The growth of primary carbides $(Cr,Fe)_7C_3$ was suppressed as the undercooling of the solid–liquid interface decreased. Consequently, the size of the primary carbides $(Cr,Fe)_7C_3$ decreased with increasing carbon content in the deposited alloys.

Fig. 6 shows the hardness of samples with different compositions of the alloying system and thus different carbon content. With an increase in the graphite addition from 10 to 20 wt.% (according to Table), hardness increased from 57 to 64 HRC. The measurement error of the macrohardness values did not exceed 1–2 HV.

Fig. 6, *b* shows that powder mixture composition **3** (Table, at a current of 100 A) makes it possible to obtain chromium carbides evenly distributed in a durable and ductile eutectic matrix $(Cr,Fe)_7C_3$ / **γ**-*Fe*. A uniform hardness distribution is observed throughout the alloyed layer, with the exception of the area near the fusion line. In this region, the density of primary $(Cr,Fe)_7C_3$ carbides is relatively low, and as a consequence, the hardness decreases sharply.

It is known [6–17] that resistance to abrasive wear is related to the hardness of materials. Prior to testing, all samples after alloying with the compositions in Table were carefully ground to a roughness of ***Ra*** < 1.25 μm. Analytical balances with an accuracy of 0.001 g were used to assess mass loss. At least three samples were tested for each coating material. After the tests, the relative wear resistance was calculated according to the formula given in [14–19]. Fig. 7 shows the mass loss during abrasive wear of chromium-

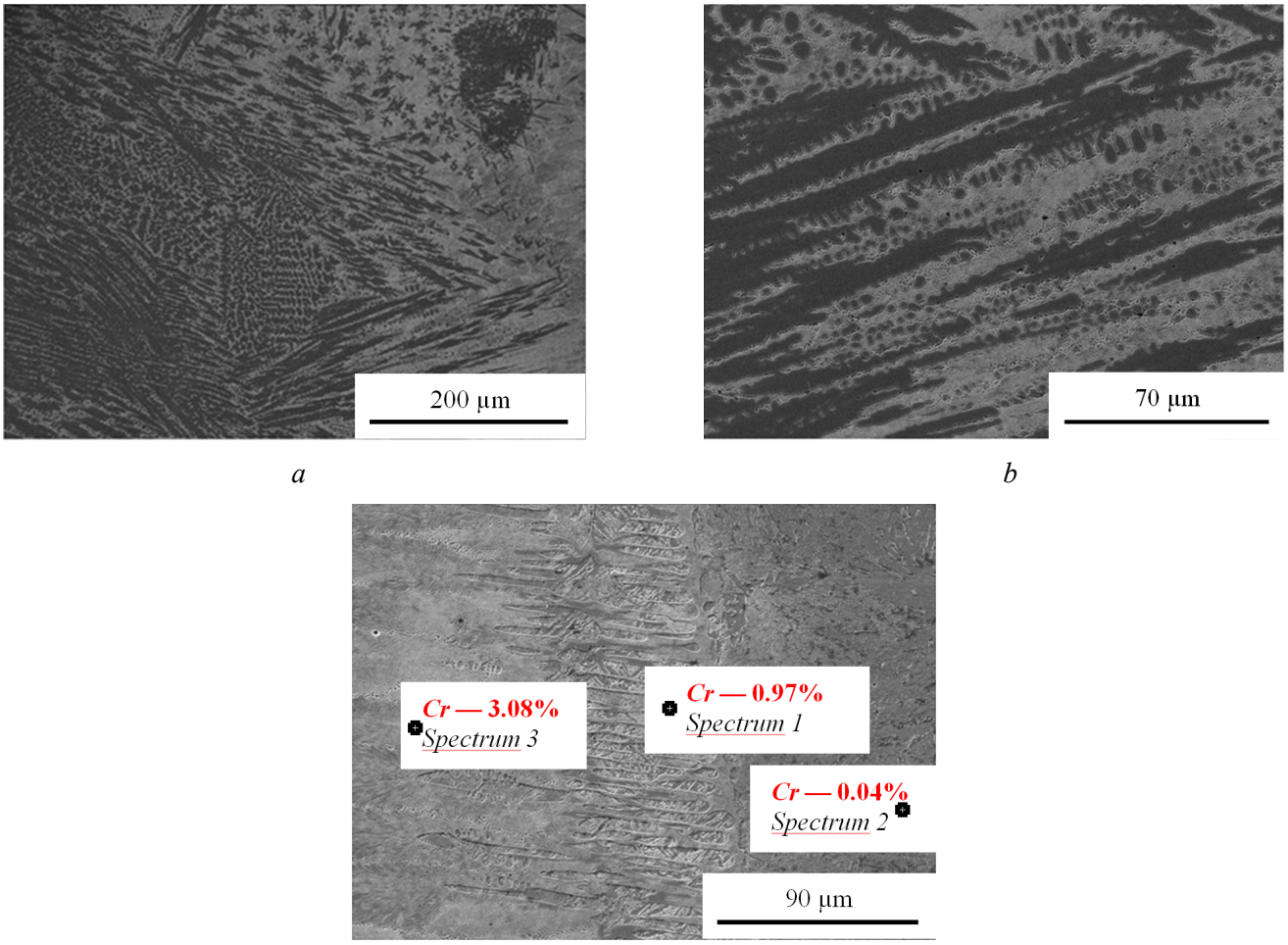

a *b* *c*

Fig. 5. Microstructures of hardening coatings with different graphite additions to the filler material:
a, *b* – electron microscopy images of primary $(Cr,Fe)_7C_3$ carbides and eutectic colonies; *c* – mass fraction of chromium in carbide phases as determined by energy-dispersive spectral analysis

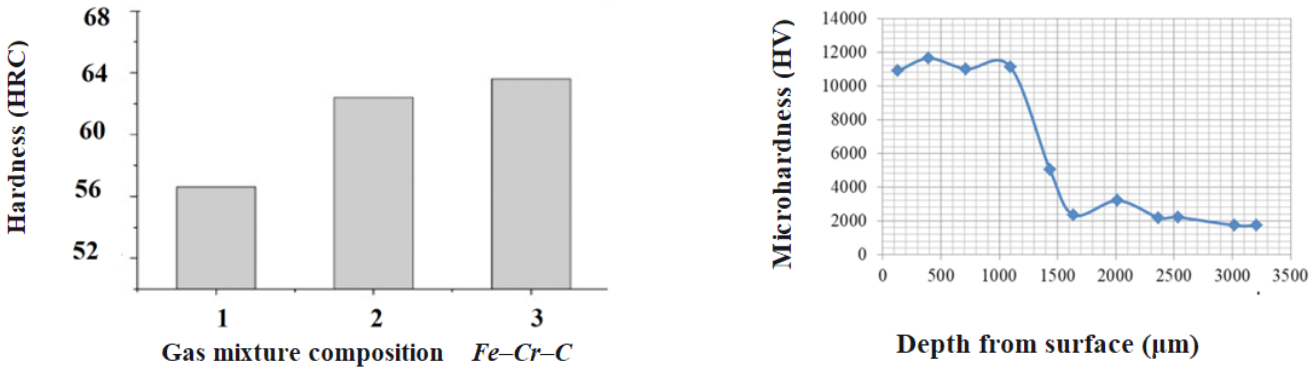

a *b*

Fig. 6. Macrohardness measured on the surface (*a*) and microhardness measured along the depth (*b*) of the alloyed layer

alloyed samples with different carbon contents. This result indicates that the mass loss decreases with increasing carbon content. A larger volume fraction of primary carbides can prevent abrasive particles from damaging the eutectic colonies. Consequently, an increase in the carbon content in the alloying powder mixture (Table) can improve the wear resistance of the alloyed surface layer consisting of a *Fe–Cr–C* composition.

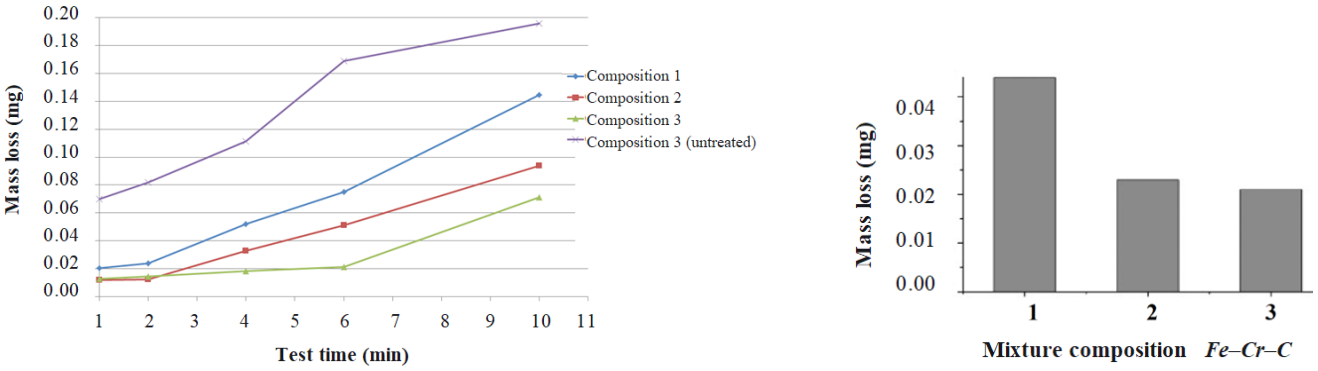

a *b*

Fig. 7. Abrasive wear resistance of samples with different *Fe–Cr–C* mixture compositions:

a – test results under a load of 10 N for samples with different carbon contents; *b* – overall wear resistance based on all test results

During testing, observation of the worn surface after the abrasive wear test indicates that the scratches caused by abrasive particles gradually became shallower with increasing carbon content in the *Fe–Cr–C* alloy. The hardness of primary $(Cr,Fe)_7C_3$ (about 1,600 HV) is higher than that of quartz (1,000–1,100 HV); therefore, primary $(Cr,Fe)_7C_3$ effectively resists damage from abrasive particles. Consequently, a higher amount of $(Cr,Fe)_7C_3$ carbides led to discontinuous scratches. In addition, craters were found on the worn surface. The formation of craters is explained by the fracture of carbides. Consequently, the number of craters increased with an increase in the proportion of primary carbides. In addition to the above, we note that micro-ploughing wear caused by abrasive particles leads to significant deformation of the matrix, forming pile-ups along the edges of the grooves. The grooves become narrower and shallower as the abrasive particles encounter the carbides. A higher proportion of carbides on the surface leads to the disappearance of plastic pile-ups. Craters are also present on the worn surface of each coating. The formation of craters occurs due to the continuous impact of abrasive particles on carbides, causing their fracture and pull-out.

Discussion of the results

During the assessment of the heat content of the welding arc burning in a mixture of gases, an increase in arc voltage was observed. This is due to the fact that the chemical reactivity of the shielding gas, the ionization potential**,** and thermal conductivity are key factors. Argon has a higher ionization energy (15.8 eV) than CO_2 (13.8 eV); a gas mixture with a lower ionization potential increases arc stability, reduces voltage, and affects the penetration depth. Thermal conductivity also affects the shape of the arc, the temperature distribution, and the depth of penetration [16, 17]. The thermal conductivity of CO_2 (3.32×10^{-5} cal/(cm×s×°C)) is significantly higher than that of argon (0.406×10^{-5} cal/(cm×s×°C)); the addition of CO_2 to argon creates a hotter, more focused arc, transferring more heat energy to the workpiece [11–17]. Despite the lower ionization potential of $\mathbf{CO_2}$, its molecular structure (*O=C=O*) makes it more reactive in high-temperature arcs. Although CO_2 has a lower ionization potential than *Ar*, it dissociates into *CO* and O_2 in the arc. Oxygen, being electronegative, captures free electrons, reducing the total electron density and increasing electrical resistance (since conductivity is proportional to electron density). This leads to a higher arc voltage at a given current, affecting heat generation, penetration, and microstructure. The addition of up to 20% CO_2 increases the arc voltage, despite the lower average ionization potential, due to several factors.

First, CO_2 requires energy to dissociate into carbon and oxygen, which are removed from the arc, increasing the effective voltage needed to maintain ionization.

Secondly, CO_2 has a higher thermal conductivity than argon, which leads to greater heat loss at the periphery of the arc, causing the arc to constrict and the current density to increase, which requires a higher

voltage for the same current. Finally, CO_2 changes the plasma composition by introducing oxygen **(O^-)** ions, which increase the arc resistance, further increasing the voltage. These combined effects lead to the fact that CO_2 in shielding gases provides a greater heat supply (due to high temperature and, as a result, energy density) compared with pure argon [15–17].

In accordance with metallographic observations, a wide range of microhardness values was measured in samples coated with a *Fe–Cr–C* mixture according to Table 1. Microhardness values from 550 to 1,270 $HV_{0.2}$ were obtained, which is due to the different carbon-to-chromium ratio in the powder mixture. The maximum microhardness value of 1,570 $HV_{0.2}$ was obtained with composition **3**. In this context, it should be noted that the microhardness of the base metal is 200 $HV_{0.2}$; i.e., approximately at least a fourfold increase in surface hardness was achieved.

It is known that experiments on surface carburizing of the same steel yielded a maximum hardness of 900–1,000 $HV_{0.2}$ [16–19]. Thus, the even higher hardness obtained in our work indicates the formation of chromium carbides on the steel surface. The presented results show that during the formation of multicomponent metal surface layers, several main phases can simultaneously form, differing in morphology, elemental and phase compositions, and the type and parameters of the crystal lattice. It is known that the cooling and crystallization of the melt in the weld pool occur at a high rate. Due to the short duration of the melt's existence and the resulting high local heterogeneity in the concentration of components, phase formation processes most often do not reach completion, and most reactions in the re-melted zone of the alloying paste and metal do not reach a fully equilibrium state, including one characterized by a uniform distribution of the elemental composition within the formed phases. All the main phases found in the work are characterized by heterogeneity of the elemental composition and parameters of the crystal lattice. However, taking into account these features, the structural and phase state of the coating can be considered "quasi-equilibrium", since additional external influences (temperature, pressure, etc.) are required to change its parameters. These features require the development of approaches to the description of the complex structural and phase state and the corresponding physical and mechanical properties. In fact, the resulting state can be represented as a complex structural-phase composite. The fact that the microhardness values of the coating vary significantly at different distances from the surface indicates the graded nature of the structural and phase state of such a composite. In this case, HV actually makes it possible to determine the integral microhardness values of the layer formed by the *Fe–Cr–C* alloying system, taking into account the resulting indentation sizes (10 to 15 μm). Different composite elements in various proportions fall within the area of interaction with the indenter.

Studies by the authors [6–18] report that primary M_7C_3 carbides are classified into two morphologies, including rod-shaped and blade-shaped forms in *Fe–Cr–C* systems. In Fig. 5, the morphology of primary $(Cr,Fe)_7C_3$ changes from blade-shaped to rod-shaped, depending on the carbon content in the coating (Table). The morphology of solidification and the growth pattern of the alloyed metal are controlled by the thermal conditions of the weld pool [17]. The formation and growth of primary $(Cr,Fe)_7C_3$ carbides during the solidification process occur with their long axes parallel to the direction of the heat flow. With a lower carbon content, the number of nucleation sites of primary $(Cr,Fe)_7C_3$ carbides decreases, and the direction of their growth becomes random. The primary rods of $(Cr,Fe)_7C_3$ carbide appear blade-like when their axes are perpendicular to the observation surface. With an increase in the carbon content in the coating composition (Table 1), the number of nucleation sites of primary carbides increases and the morphology changes from rod to blade. As the temperature decreases, eutectic colonies appear around the primary grain boundaries $(Cr,Fe)_7C_3$, as shown in Fig. 5. Consequently, these phases have a hypereutectic structure containing primary $(Cr,Fe)_7C_3$ and eutectic colonies of austenite + $(Cr,Fe)_7C_3$.

In addition, the surface fraction of carbides according to [6–17] increased from 33.8 to 86.1% with an increase in the carbon content from 3.73 to 4.85 wt.%. For a non-eutectic composition, the liquidus temperature of the alloy is significantly higher than the eutectic temperature. Thus, the corresponding primary phase, which experiences greater undercooling, tends to grow faster than the eutectic [6–10]. A comparison of Fig. 4, *a*, *b* shows that an increase in the carbon content contributes to the formation of primary $(Cr,Fe)_7C_3$ carbides. The addition of carbon reduced the eutectic temperature of the *Fe–Cr–C* alloy

[21]. A lower eutectic temperature leads to a decrease in the number of eutectic colonies. Therefore, the addition of carbon promotes the formation of primary *(Cr,Fe)$_7$C$_3$* carbides but suppresses the growth of eutectic colonies.

Analyzing the results of the abrasive wear tests obtained, we note the following. Wear usually depends on the ratio of the hardness of the abrasive particles and the material. An abrasive particle is called "hard" if its hardness is about 20 % greater than the hardness of the material being tested in the worn state [6–12]. Hard abrasive particles easily plough small phases and cut or split larger ones. Soft abrasive particles can plough small phases or form large craters [15]. According to [1, 2], if the hardness of the hardening particles is lower than the hardness of the abrasive particles, the particles are pulled out of the matrix or are fractured by the action of abrasive particles. Soft abrasives cannot indent the surface of the material, and adhesion and contact fatigue occur as the predominant wear mechanisms, accompanied by greater or lesser plastic deformation [8–10]. In this case, the hardness of quartz sands (1,000–1,100 HV) is lower than that of rod-shaped *(Cr,Fe)$_7$C$_3$* carbides (1,300–1,350 HV) but higher than that of eutectic colonies (750–800 HV). The hardness of blade-shaped *(Cr,Fe)$_7$C$_3$* carbides is also similar to that of quartz particles. In this study, the relative hardness of quartz particles of abrasive paper relative to eutectic colonies is about 1.25. Quartz particles are harder than eutectic colonies, so they easily destroy eutectic colonies. The relative hardness of quartz particles relative to rod-shaped *(Cr,Fe)$_7$C$_3$* carbides is about 0.75. Quartz particles are soft abrasive particles for primary *(Cr,Fe)$_7$C$_3$* carbides, which are difficult to indent or plough. The relative hardness of quartz particles relative to blade-shaped *(Cr,Fe)$_7$C$_3$* carbides is about 0.91. Blade-shaped *(Cr,Fe)$_7$C$_3$* carbides have less resistance to indentation or ploughing by quartz particles than rod-shaped ones. Based on the research results, we offer the following explanation of the effect of the carbide content on the wear mechanism. The surface fraction of carbides increases with increasing carbon content. This is confirmed by the data of X-ray diffraction analysis (Fig. 4, 5). In addition, carbides in the form of blades are found in the structure of a layer with a lower carbon content, and carbides in the form of rods are found in an area with a higher carbon content [8, 10, 15–18]. Firstly, when carbides are present in composition No. 1, abrasive particles form microgrooves in eutectic colonies, causing their destruction. Plastic grooves and craters appear on the worn surface. Continuous damage by abrasive particles gradually leads to the exposure of harder blade-shaped *(Cr,Fe)$_7$C$_3$* carbides due to their higher hardness. Eventually, the morphology of the craters takes on a polygonal shape. The formation of craters is explained by the fracture and pull-out of carbides. As the surface fraction of carbides in composition No. 2 increases, the plastic grooves gradually disappear. Rod-shaped *(Cr,Fe)$_7$C$_3$* carbides are sufficient to protect eutectic colonies. Finally, the mechanism of wear of samples of composition No. 3 consists of the fracture or pull-out of carbides when the surface fraction of carbides is 86.1%. Dense *(Cr,Fe)$_7$C$_3$* carbides prevent the formation of eutectic colonies under the influence of quartz particles. However, quartz particles accumulate and attack dense *(Cr,Fe)$_7$C$_3$* carbides, causing their fracture and pull-out. Repeated exposure to quartz particles leads to the fact that *(Cr,Fe)$_7$C$_3$* carbides resist abrasive action until they fracture and are pulled out of the metal matrix.

Many authors note that there is a relationship between the proportion of carbides on the surface and wear resistance [8–16]. The results of the work of these authors show that an increase in the proportion of carbides on the surface improves the wear resistance of the coating. This is due to the fact that the increased content of hard primary *(Cr,Fe)$_7$C$_3$* carbides provides a barrier against indentation, grooving, and cutting by abrasive particles. Our results show that the relationship between wear resistance and the proportion of carbides on the surface is nonlinear. Wear resistance increases rapidly with an increase in the proportion of carbides on the surface. Therefore, wear resistance depends not only on the proportion of carbides on the surface and hardness. It should be understood that from a physical perspective, the abrasive particles should be small enough to fit between the carbide rods so that they can penetrate deeper into the matrix and push the carbide out from behind. If the abrasive particles are "large" compared to the distance between the carbides, the abrasive particles will slide over the carbides without penetrating significantly into the matrix [6–8, 16–19]. Thus, the mean free path between carbides also affects wear resistance. We assume that the combination of hardness and mean free path is the main factor in wear resistance. In our further research, we will continue our work with other alloying systems for surface layers of steel.

Conclusion

Thus, our research has shown that in this process of surface alloying using gas tungsten arc welding (*GTAW*), the shape and size of the fusion zone on the surface of the steel are determined by the arc parameters, such as current, voltage, and travel speed, while the molten metal pool is protected from atmospheric contamination by inert argon shielding gas. The addition of carbon dioxide to the shielding gas increases the heat input of the welding arc and ensures the completeness of the metallurgical reactions in the molten pool. To form a series of hypereutectic solid alloyed surface layers using the *Fe–Cr–C* system, compositions with different carbon contents were developed to study their microstructure, wear resistance, and wear mechanism. A summary of the results is provided below:

1. It was found that the addition of carbon dioxide to argon shielding gas in the range of 5–10% increases the heat content of the welding arc, resulting in a voltage increase of 4–5 V; this increases the penetration capacity of the welding arc by 30–50%.

2. The alloyed surface layer on *St3* steel consists of a primary phase $(Cr,Fe)_7C_3$ and a small amount of interdendritic eutectic $(Cr,Fe)_7C_3$ / **γ**-*Fe*. It is shown that a feature of the alloyed layer is the presence of large primary $(Cr,Fe)_7C_3$ carbides, evenly distributed in a fine-grained, strong, and ductile eutectic matrix $(Cr,Fe)_7C_3$ / **γ**-*Fe*, which ensures a high and uniform hardness distribution. The maximum hardness of 1,570 $HV_{0.2}$ of the surface layer alloyed with the *Fe–Cr*–C system using a composition of 20% graphite and 80% chromium oxide was obtained, which is due to the presence of massive hard $(Cr,Fe)_7C_3$ carbides.

3. As the carbon content of the saturating coating increases, the proportion of chromium carbides increases. Chromium carbides in the form of blades are found in coatings with a lower carbon content, while chromium carbides in the form of rods are found in those with a higher carbon content. Abrasive wear resistance depends not only on the surface fraction of carbides, but also on the hardness of the deposited layer and the mean free path between carbides. An increase in the surface fraction of carbides increases wear resistance and leads to the disappearance of plastic ploughing. The formation of craters is also associated with the fracture and pull-out of carbides.

References

1. Mendez P.F., Barnes N., Bell K., Borle S.D., Gajapathi S.S., Guest S.D., Izadi H., Gol A.K., Wood G. Welding processes for wear resistant overlays. *Journal of Manufacturing Processes*, 2014, vol. 16 (1), pp. 4–25. DOI: 10.1016/j.jmapro.2013.06.011.

2. Kanishka K., Acherjee B. A systematic review of additive manufacturing-based remanufacturing techniques for component repair and restoration. *Journal of Manufacturing Processes*, 2023, vol. 89, pp. 220–283. DOI: 10.1016/j.jmapro.2023.01.034.

3. Maiorov V.S. Lazernoe uprochnenie metallov [Laser hardening of metals]. *Lazernye tekhnologii obrabotki materialov: sovremennye problemy fundamental'nykh issledovanii i prikladnykh razrabotok* [Laser technologies of materials processing: modern problems of fundamental research and applied developments]. Moscow, Fizmatlit Publ., 2009, pp. 439–469.

4. Poletika I.M., Golkovskii M.G., Perovskaya M.B. Elektronno-luchevaya zakalka poverkhnostnogo sloya stali vne vakuuma [Electron-beam hardening of steel surface layer outside vacuum]. *Fizicheskaya mezomekhanika = Physical Mesomechanics*, 2006, no. 9, pp. 181–184. DOI: 10.24411/1683-805X-2006-00026.

5. Balanovsky A.E. Osnovnye voprosy teorii plazmennogo poverkhnostnogo uprochneniya metallov (Obzor. Ch. 1) [The main problems in the theory of plasma surface hardening of metals (Review. Part 1)]. *Uprochnyayushchie tekhnologii i pokrytiya = Strengthening Technologies and Coatings*, 2015, no. 12, pp. 18–30.

6. Balanovsky A.E. Uprochnenie poverkhnosti katoda pri vzaimodeistvii s katodnymi pyatnami dugovogo razryada [The hardening of a cathode surface under conditions of interaction with cathode spots of arc discharge]. *Teplofizika vysokikh temperatur = High Temperature*, 1993, vol. 31, no. 2, pp. 328–330. (In Russian).

7. Losinskaya A.A., Drobyaz E.A., Bataev V.A., Plotnikova N.V., Golkovsky M.G. Struktura i svoistva poverkhnostnykh sloev nizkouglerodistoi stali, poluchennykh metodom naplavki uglerodsoderzhashchikh poroshkovykh smesei i posleduyushchei zakalki [Structure and properties of the low carbon steel surface layers, obtained by cladding of carbon-containing powder mixtures, followed by quenching]. *Obrabotka metallov (tekhnologiya, oborudovanie, instrumenty) = Metal Working and Material Science*, 2013, no. 4 (61), pp. 5–11.

8. Losinskaya A.A., Golovin D.D. Formirovanie vysokouglerodistykh sloev na stali i ikh zakalka s ispol'zovaniem moshchnogo elektronnogo puchka, vyvedennogo v atmosferu [Formation of high-carbon layers on steel and its hardening using a powerful electron beam led out to the atmosphere]. *Perspektivy nauki = Science Prospects*, 2013, no. 10 (49), pp. 7–10.

9. Dampilon B.V., Durakov V.G., Eremina L.V., Losinskaya A.A., Mochalina N.S. Svoistva zashchitnykh pokrytii iz evtekticheskogo khromovanadievogo chuguna, poluchennykh elektronno-luchevoi naplavkoi v vakuume [Properties of protective coatings on the base of eutectic chrome-vanadium iron obtained by electron-beam hardfacing in vacuum]. *Obrabotka metallov (tekhnologiya, oborudovanie, instrumenty) = Metal Working and Material Science*, 2011, no. 3 (52), pp. 80–84.

10. Bataev I.A., Kurlaev N.V., Butylenkova O.A., Lenivtseva O.G., Losinskaya A.A. Morfologiya boridov zheleza v poverxnostnom sloe, naplavlennom èlektronnym luchom [Morphology of iron borides in coatings, produced by non-vacuum electron beam cladding] *Obrabotka metallov (tekhnologiya, oborudovanie, instrumenty) = Metal Working and Material Science*, 2012, no. 1 (54), pp. 85–89.

11. Bataev I.A., Bataev A.A., Golkovski M.G., Krivizhenko D.S., Losinskaya A.A., Lenivtseva O.G. Structure of surface layers produced by non-vacuum electron beam boriding. *Applied Surface Science*, 2013, vol. 284, pp. 472–481. DOI: 10.1016/j.apsusc.2013.07.121.

12. Mul D.O., Drobyaz E.A., Chakin I.K., Samoylenko V.V., Lozhkin V.S., Dostovalov R.A. Struktura i svoistva stali posle vnevakuumnoi elektronno-luchevoi naplavki poroshkov titana, tantala, molibdena i grafita [Structure and properties of steel under non-vacuum electron-beam welding deposition of titanium, tantalum, molybdenum and graphite powders]. *Obrabotka metallov (tekhnologiya, oborudovanie, instrumenty) = Metal Working and Material Science*, 2013, no. 3 (60), pp. 115–120.

13. Mul D.O., Belousova N.S., Krivezhenko D.S., Shevtsova L.I., Losinskaya A.A. Elektronno-luchevaya naplavka titan- i tantalsoderzhashchikh poroshkovykh smesei na obraztsy iz stali X [Electron beam cladding of powder mixtures containing titanium and tantalum on specimens of steel 40X]. *Obrabotka metallov (tekhnologiya, oborudovanie, instrumenty) = Metal Working and Material Science*, 2014, no. 2 (63), pp. 117–126. DOI: 10.17212/1994-6309-2020-22.2-89-103.

14. Zimogliadova T.A., Bushueva E.G., Shtertser A.A., Grinberg B.E., Soboleva N.N., Kollmannsberger E., Chakin I.K., Bibko D.S., Leonov A.V., Safarova D.E. Strukturnye osobennosti i iznosostoikost' sloev, sformirovannykh naplavkoi samoflyusuyushchegosya nikelevogo splava i bora elektronnym luchom, vyvedennym v vozdushnuyu atmosferu [Structure features and wear resistance of layers, formed by Ni-based self-fl uxing alloy combined with boron by electron beam, revealed in the air atmosphere]. *Obrabotka metallov (tekhnologiya, oborudovanie, instrumenty) = Metal Working and Material Science*, 2020, vol. 22, no. 2, pp. 89–103. DOI: 10.17212/1994-6309-2020-22.2-89-103.

15. Balanovsky A.E., Vu Van Guy. Tekhnologicheskoe povyshenie kachestva poverkhnosti detalei s plazmennoi tsementatsiei [Technological quality increase in surfaces of parts with plasma carbonization]. *Naukoemkie tekhnologii v mashinostroenii = Science Intensive Technologies in Mechanical Engineering*, 2017, no. 3 (69), pp. 16–24. DOI: 10.12737/24960.

16. Balanovsky A.E., Grechneva M.V., Vu Van Guy. Issledovanie struktury rel'sovoi stali posle plazmennogo poverkhnostnogo uprochneniya [Study of the structure of rail steel after plasma surface hardening]. *Uprochnyayushchie tekhnologii i pokrytiya = Strengthening Technologies and Coatings*, 2015, no. 11 (131), pp. 23–32.

17. Balanovsky A.E., Wu W.G. Nasyshchenie poverkhnosti metalla uglerodom pri plazmennoi poverkhnostnoi obrabotke [Carburization of the metal surface by plasma surface treatment]. *Uprochnyayushchie tekhnologii i pokrytiya = Strengthening Technologies and Coatings*, 2017, vol. 13, no. 9 (153), pp. 403–415.

18. Vu Van Huy, Balanovsky A.E. Issledovanie iznosostoikosti poverkhnosti stali posle plazmennoi tsementatsii s ispol'zovaniem uglerodosoderzhashchei pasty [Studying steel surface wear resistance after carbonaceous paste-employing plasma carburizing]. *Vestnik Irkutskogo gosudarstvennogo tekhnicheskogo universiteta = Proceedings of Irkutsk State Technical University*, 2017, vol. 21, no. 4, pp. 10–21. DOI: 10.21285/1814-3520-2017-4-10-21.

19. Vu Van Huy, Balanovsky A.E. Fizicheskie osnovy tekhnologii plazmennoi poverkhnostnoi tsementatsii detalei na primere vtulki shpintona passazhirskogo vagona [Physical principles of plasma surface carburizing of parts as exemplified by an antirattle bushing of a passenger coach]. *Vestnik Irkutskogo gosudarstvennogo tekhnicheskogo universiteta = Proceedings of Irkutsk State Technical University*, 2017, vol. 21, no. 3, pp. 10–22. DOI: 10.21285/1814-3520-2017-3-10-22.

20. Balanovskii A., Vu V. Plazmennaya poverkhnostnaya tsementatsiya s ispol'zovaniem grafitovogo pokrytiya [Plasma surface carburizing with graphite paste]. *Pis'ma o materialakh = Letters on Materials*, 2017, vol. 7, no. 2 (26), pp. 175–179. DOI: 10.22226/2410-3535-2017-2-175-179.

21. Tsai N.S., Eagar T.W. Distribution of the heat and current fluxes in gas tungsten arcs. *Metallurgical transactions B*, 1985, vol. 16 (4), pp. 841–846. DOI: 10.1007/BF02667521.

22. Yüksel N., Şahin S. Wear behavior–hardness–microstructure relation of Fe–Cr–C and Fe–Cr–C–B based hardfacing alloys. *Materials & Design*, 2014, vol. 58, pp. 491–498. DOI: 10.1016/j.matdes.2014.02.032.

23. Kumar S., Ramakrishna A., Madugula N.S., Kumar N., Kapoor M., Bhatia H.S. Evolution of surface morphology and mechanical characterization of GTAW welded SDSS thin sheets. *Results in Surfaces and Interfaces*, 2025, vol. 18, p. 100412. DOI: 10.1016/j.rsurfi.2024.100412.

24. Gong T.Z., Chen Y., Hao W.Y., Chen X.Q., Li D.Z. Modeling segregation of Fe–C alloy in solidification by phase-field method coupled with thermodynamics. *Metals*, 2023, vol. 13 (6), p. 1148. DOI: 10.3390/met13061148.

25. Xu C., Chen Y., Gong T., Shi Y., Wang J., Chen X., Liu P., Guo Y., Li D. Ab initio study of local structures during cooling of liquid Fe-C and Fe-Cr-C alloys. *Computational Materials Science*, 2022, vol. 212, p. 111572. DOI: 10.1016/j.commatsci.2022.111572.

26. Atamert S., Bhadeshia H.K.D.H. Microstructure and stability of Fe-Cr-C hardfacing alloys. *Materials Science and Engineering: A*, 1990, vol. 130 (1), pp. 101–111. DOI: 10.1016/0921-5093(90)90085-H.

27. Kluczyński J., Jasik K., Łuszczek J., Pokropek J. Laser surface hardening of carburized steels: A review of process parameters and application in gear manufacturing. *Materials*, 2025, vol. 18 (15), p. 3623. DOI: 10.3390/ma18153623.

28. Łach Ł. Recent advances in laser surface hardening: techniques, modeling approaches, and industrial applications. *Crystals*, 2024, vol. 14 (8), p. 726. DOI: 10.3390/cryst14080726.

29. Maharjan N., Zhou W., Zhou Y., Wu N. Decarburization during laser surface processing of steel. *Applied Physics A*, 2018, vol. 124 (10), p. 682. DOI: 10.1007/s00339-018-2104-5.

30. Konstantinova M.V., Balanovskiy A.E., Gozbenko V.E., Kargapoltsev S.K., Karlina A.I., Shtayger M.G., Guseva E.A., Kuznetsov B.O. Application of plasma surface quenching to reduce rail side wear. *IOP Conference Series: Materials Science and Engineering*, 2019, vol. 560 (1), p. 012146. DOI: 10.1088/1757-899X/560/1/012146.

31. Kondratiev V.V., Karlina A.I., Guseva E.A., Konstantinova M.V., Kleshnin A.A. Processing and application of ultra disperse wastes of silicon production in construction. *IOP Conference Series: Materials Science and Engineering*, 2018, vol. 463 (3), p. 032068. DOI: 10.1088/1757-899X/463/3/032068.

32. Balanovsky A.E., Shtayger M.G., Kondrat'ev V.V., Nebogin S.A., Karlina A.I. Complex metallographic researches of 110G13L steel after heat treatment. *IOP Conference Series: Materials Science and Engineering*, 2018, vol. 411 (1), p. 012014. DOI: 10.1088/1757-899X/411/1/012014.

33. Balanovsky A.E., Shtayger M.G., Grechneva M.V., Kondrat'ev V.V., Karlina A.I. Comparative metallographic analysis of the structure of St3 steel after being exposed to different ways of work-hardening. *IOP Conference Series: Materials Science and Engineering*, 2018, vol. 411 (1), p. 012012. DOI: 10.1088/1757-899X/411/1/012012.

34. Ivanchik N.N., Balanovsky A.E., Shtayger M.G., Sysoev I.A., Karlina A.I. Capability enhancement of production of activating fluxes for arc welding using ultradispersed products of silicon waste processing. *IOP Conference Series: Materials Science and Engineering*, 2018, vol. 411 (1), p. 012035. DOI: 10.1088/1757-899X/411/1/012035.

35. Adigamov R.R., Baraboshkin K.A., Mishnev P.A., Karlina A.I. Development of rolling procedures for pipes of K55 strength class at the laboratorial mill. *CIS Iron and Steel Review*, 2022, vol. 24, pp. 60–66. DOI: 10.17580/cisisr.2022.02.09.

36. Yelemessov K., Baskanbayeva D., Martyushev N.V., Skeeba V.Y., Gozbenko V.E., Karlina A.I. Change in the properties of rail steels during operation and reutilization of rails. *Metals*, 2023, vol. 13, p. 1043. DOI: 10.3390/met13061043.

37. Balanovskiy A.E., Shtaiger M.G., Kondratyev V.V., Karlina A.I. Determination of rail steel structural elements via the method of atomic force microscopy. *CIS Iron and Steel Review*, 2022, vol. 23, pp. 86–91. DOI: 10.17580/cisisr.2022.01.16.

38. Kondrat'ev V.V., Gorovoy V.O., Kolosov A.D., Kononenko R.V., Konyukhov V.Y. Description of the complex of technical means of an automated control system for the technological process of thermal vortex enrichment. *Journal of Physics: Conference Series*, 2020, 1661(1), 012101, DOI: 10.1088/1742-6596/1661/1/012101.

39. Karlina A.I., Balanovskiy A.E., Kondratiev V.V., Romanova V.V., Batukhtin A.G., Karlina Y.I. An investigation into the behavior of cathode and anode spots in a welding discharge. *Applied Sciences Switzerland*, 2024, vol. 14 (21), p. 9774. DOI: 10.3390/app14219774.

40. Karlina A.I., Kondratyev V.V., Balanovskiy A.E., Astafyeva N.A. Checking of convergence of the finite element model for the software complex Simufact Welding with the real experiment using the method of additive manufacturing WAAM. *CIS Iron and Steel Review*, 2025, vol. 29, pp. 82–88. DOI: 10.17580/cisisr.2025.01.15.

41. Karlina A.I., Kondratyev V.V., Gozbenko V.E., Kononenko R.V. Study of hardness distribution in a rail welded joint after welding with accelerated cooling. *CIS Iron and Steel Review*, 2024, vol. 28, pp. 56–62. DOI: 10.17580/cisisr.2024.02.10.

42. Karlina A.I., Kondratyev V.V., Balanovskiy A.E., Astafyeva N.A., Yamshchikova E.A. Porosity reduction in metal with hybrid wire and arc additive manufacturing technology (WAAM). *CIS Iron and Steel Review*, 2024, vol. 27, pp. 91–95. DOI: 10.17580/cisisr.2024.01.14.

43. Skeeba V.Yu., Ivancivsky V.V., Kutyshkin A.V., Parts K.A. Hybrid processing: The impact of mechanical and surface thermal treatment integration onto the machine parts quality. *IOP Conference Series: Materials Science and Engineering*, 2016, vol. 126 (1), p. 012016. DOI: 10.1088/1757-899x/126/1/012016.

44. Efremenkov E.A., Martyushev N.V., Skeeba V.Yu., Grechneva M.V., Olisov A.V., Ens A.D. Research on the possibility of lowering the manufacturing accuracy of cycloid transmission wheels with intermediate rolling elements and a free cage. *Applied Sciences*, 2022, vol. 12 (1), p. 5. DOI: 10.3390/app12010005.

45. Martyushev N.V., Skeeba V.Yu. The method of quantitative automatic metallographic analysis. *Journal of Physics: Conference Series*, 2017, vol. 803 (1), p. 012094. DOI: 10.1088/1742-6596/803/1/012094.

46. Skeeba V.Yu., Ivancivsky V.V. Reliability of quality forecast for hybrid metal-working machinery. *IOP Conference Series: Earth and Environmental Science*, 2018, vol. 194 (2), p. 022037. DOI: 10.1088/1755-1315/194/2/022037.

47. Kenjaev B., Paluanov D., Mamatkulov D., Romanova V. Methods and technologies for ensuring the reliability of excitation of synchronous generators of small hydroelectric power stations in Uzbekistan. *E3S Web of Conferences*, 2020, vol. 216, p. 01065. DOI: 10.1051/e3sconf/202021601065.

48. Solonina N., Suslov K., Solonina Z., Romanova V. Advanced approach to compensation of reactive power in isolated arctics electrical supply systems. *Journal of Physics: Conference Series*, 2021, vol. 2032 (1), p. 012113. DOI: 10.1088/1742-6596/2032/1/012113.

49. Romanova V., Khromov S., Suslov K. Multi-factor analysis of external effects influencing the operational reliability of asynchronous electric motors. *E3S Web of Conferences*, 2020, vol. 216, p. 01084. DOI: 10.1051/e3sconf/202021601084.

50. Kondrat'ev V.V., Gorovoy V.O., Kolosov A.D., Kononenko R.V., Konyukhov V.Y. Description of the complex of technical means of an automated control system for the technological process of thermal vortex enrichment. *Journal of Physics: Conference Series*, 2020, vol. 1661 (1), p. 012101. DOI: 10.1088/1742-6596/1661/1/012101.

Conflicts of Interest

The authors declare no conflict of interest.